

Accepted Manuscript

Full length article

Feasible and pure P_2O_5 -CaO nanoglasses: an in-depth NMR study of synthesis for the modulation of the bioactive ion release

Joan Marti-Munoz, Elena Xuriguera, John W. Layton, Josep A. Planell, Stephen E. Rankin, Elisabeth Engel, Oscar Castano

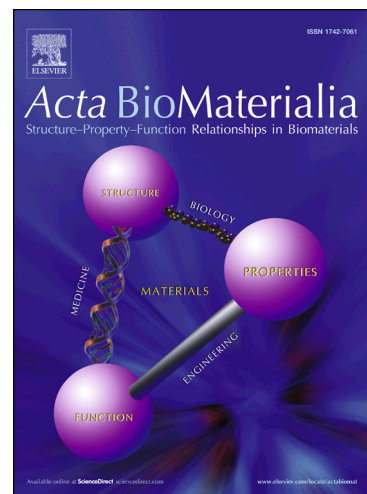
PII: S1742-7061(19)30392-7
DOI: <https://doi.org/10.1016/j.actbio.2019.05.065>
Reference: ACTBIO 6166

To appear in: *Acta Biomaterialia*

Received Date: 18 February 2019
Revised Date: 19 May 2019
Accepted Date: 24 May 2019

Please cite this article as: Marti-Munoz, J., Xuriguera, E., Layton, J.W., Planell, J.A., Rankin, S.E., Engel, E., Castano, O., Feasible and pure P_2O_5 -CaO nanoglasses: an in-depth NMR study of synthesis for the modulation of the bioactive ion release, *Acta Biomaterialia* (2019), doi: <https://doi.org/10.1016/j.actbio.2019.05.065>

This is a PDF file of an unedited manuscript that has been accepted for publication. As a service to our customers we are providing this early version of the manuscript. The manuscript will undergo copyediting, typesetting, and review of the resulting proof before it is published in its final form. Please note that during the production process errors may be discovered which could affect the content, and all legal disclaimers that apply to the journal pertain.



Feasible and pure P₂O₅-CaO nanoglasses: an in-depth NMR study of synthesis for the modulation of the bioactive ion release

Joan Marti-Munoz,^{a,b} Elena Xuriguera,^c John W. Layton,^d Josep A. Planell,^{a,b} Stephen E. Rankin,^e Elisabeth Engel,^{,a,b,f} and Oscar Castano^{*,g,a,b,h}*

^a Biomaterials for Regenerative Therapies, Institute for Bioengineering of Catalonia (IBEC), The Barcelona Institute of Science and Technology (BIST), 08028 Barcelona, Spain

^b CIBER en Bioingeniería, Biomateriales y Nanomedicina (CIBER-BBN), 28029 Madrid, Spain

^c Materials Science and Physical Chemistry Department, University of Barcelona (UB), 08028 Barcelona, Spain

^d Department of Chemistry, University of Kentucky (UKY), Lexington, KY 40506-0053, USA

^e Chemical and Materials Engineering Department, University of Kentucky (UKY), Lexington, KY 40506-0053, USA

^f Materials Science and Metallurgy Department (EEBE), Technical University of Catalonia (UPC), 08019 Barcelona, Spain

^g Serra Hunter Fellow, Electronics and Biomedical Engineering Department, University of Barcelona (UB), 08028 Barcelona, Spain

^h Institute of Nanoscience and Nanotechnology Department, University of Barcelona (UB), 08028 Barcelona, Spain

KEYWORDS: calcium phosphate glasses, sol-gel process, NMR spectroscopy, ion release, biomaterials

ABSTRACT: The use of bioactive glasses (e.g. silicates, phosphates, borates) has demonstrated to be an effective therapy for the restoration of bone fractures, wound healing and vascularization. Their partial dissolution towards the surrounding tissue has shown to trigger positive bioactive responses, without the necessity of using growth factors or cell therapy, which reduces money-costs, side effects and increases their translation to the clinics. However, bioactive glasses often need from stabilizers (e.g. SiO_4^{4-} , Ti^{4+} , Co^{2+} , etc.) that are not highly abundant in the body and which metabolization is not fully understood. In this study, we were focused on synthesizing pure calcium phosphate glasses without the presences of such stabilizers. We combined a mixture of ethyphosphate and calcium 2-methoxyethoxide to synthesize nanoparticles with different compositions and degradability. Synthesis was followed by an in-depth nuclear magnetic resonance characterization, complemented with other techniques that helped us to correlate the chemical structure of the glasses with their physiochemical properties and reaction mechanism. After synthesis, the organically modified xerogel (i.e. calcium monoethylphosphate) was treated at 200 or 350 °C and its solubility was maintained and controlled due to the elimination of organics, increase of phosphate-calcium interactions and phosphate polycondensation. To the best of our knowledge, we are reporting the first sol-gel synthesis of binary (P_2O_5 -CaO) calcium phosphate glass nanoparticles in terms of continuous poycondensated phosphate chains structure without the

addition of extra ions. The main goal is to straightforward the synthesis, to get a safer metabolization and to modulate the bioactive ion release. Additionally, we shed light on the chemical structure, reaction mechanism and properties of calcium phosphate glasses with high calcium contents, which nowadays are poorly understood.

Statement of significance

The use of bioactive inorganic materials (i.e. bioactive ceramics, glass-ceramics and glasses) for biomedical applications is attractive due to their good integration with the host tissue without the necessity of adding exogenous cells or growth factors. In particular, degradable calcium phosphate glasses are completely resorbable, avoiding the retention in the body of the highly stable silica network of silicate glasses, and inducing a more controllable degradability than bioactive ceramics. However, most calcium phosphate glasses include the presence of stabilizers (e.g. Ti^{4+} , Na^+ , Co^{2+}), which metabolization is not fully understood and complicates their synthesis. The development of binary calcium phosphate glasses with controlled degradability reduces these limitations, offering a simple and completely metabolizable material with higher transfer to the clinics.

1. INTRODUCTION

Inorganic bioactive materials in tissue regeneration, such as ceramics, glass-ceramics and glasses, are able to trigger the host cells to deliver their own biochemical cues [1] rather than introducing exogenous growth factors or cells that may interfere in a healthy metabolic state [2,3]. The release of ions such as SiO_4^{4-} , Ca^{2+} , inorganic phosphates (Pi), Cu^{2+} , Co^{2+} , Ag^+ and Zn^{2+} has demonstrated to benefit several biological processes like osteogenesis, vascularization, cell chemotaxis, wound healing or introduce antimicrobial properties [4–7]. Apart from minimizing adverse side effects, the success of inorganic bioactive materials also relies in a reduced cost and less strict regulations

to reach the market since current regulatory agencies classified the architectures involving these type of materials as a medical devices rather than drugs or biological agents [8].

Bioactive glasses (BGs) offer several advantages among inorganic bioactive materials. The main difference with bioactive ceramics (BCs) is their amorphous structure and degree of polycondensation [9,10]. These structural properties are often macroscopically correlated with a higher and more homogeneous degradation rates, which are very important for the induction of controlled and personalized bioactive resorptions. For example, it has been reported that small increases of Ti^{4+} concentration in calcium phosphate glasses (CPGs) have a high impact in the stabilization of their degradability [11]. Another characteristic is the facility to modify their composition and introduce doping agents to affect their bioactivity (e.g. angiogenic and antimicrobial agents) [4,12]. Although BCs also allow changes in their composition, the formation of stoichiometric crystalline phases limits this feature and induces heterogeneous degradability.

Despite this advantages, most BGs use doping agents with reported side effects (e.g. Ti^{4+} , Co^{2+} , Cu^{2+}) [13–15] or which metabolization is not fully understood (SiO_4^{4-}) [16]. For example, Ti^{4+} , used to stabilize CPGs, has been reported to have mutagenic effects in the wear debris of multiple hip prosthesis [13], and in the case of the widely used silicate glasses, some authors maintain that the body is not able to eliminate its highly stable silica network (SiO_2) [16,17]. It is for this reason that in the last decades, more compatible and completely resorbable glasses such as CPGs, are gaining relevance in the field of tissue regeneration and regenerative medicine [10].

CPGs are mainly composed by a condensed phosphate network containing calcium ions (Ca^{2+}) that stabilizes the structure and properties of the network itself [10]. In order to maintain the connectivity of the P_2O_5 network and avoid its disruption into smaller subunits, low amounts of Ca^{2+} and other cations have been used in the synthesis of CPGs to date [10,11,18]. However, the

significant environmental acidification due to the degradation of high amounts of P_2O_5 , has forced the use of stabilizers (e.g. Ti^{4+}) or potential basifying cations (e.g. Na^+) to smooth this effect. This has led to the formation of ternary (e.g. P_2O_5 -CaO- Na_2O), quaternary (TiO_2 - P_2O_5 -CaO- NaO) and even more complex systems difficult to synthesize, and at the same time a lack of information about CPGs with $CaO > 50\%$ [10]. Apart from Ca^{2+} cations, the phosphate network allows the incorporation of other cations (e.g. Ti^{4+} , Na^+ , Co^{2+} , etc.) [11,19,20] and even anions (e.g. F^-) [10] to tailor its degradability and other biological properties

Synthesis methods for BGs include the melt-quenching technique (top-down) and the sol-gel process (bottom-up). While melt-quenching uses high temperatures (above the melting point of metal oxides, $>1000^\circ C$) to avoid crystallization and thus achieve amorphous structures by a fast quenching, the sol-gel method uses chemical condensation of metal alkoxides in solution at low temperatures [21]. The low temperature synthesis in the sol-gel process, apart from reducing energy related costs, also allows the nanostructuring of the glasses into for example nanoparticles or foams [22,23]. This last feature has increased the popularity of the sol-gel method in tissue engineering where the interaction with the host tissue microenvironment at the nanoscale is crucial.

In this study, we were focused on developing pure CPGs (i.e. binary (P_2O_5 -CaO) CPGs) nanoparticles with different P/Ca ratios and controlled degradability. We avoid the addition of extra ions to promote a higher biocompatibility, a straightforward synthesis and at the same time elucidate the chemical structure, reaction mechanisms, and properties of CPGs with high CaO contents. A mixture of ethylphosphate and calcium 2-methoxyethoxide were used as sol-gel precursors since these two precursors have shown high affinity and the formation of glasses with homogeneous compositions [22,24,25]. Particle synthesis was followed by an exhaustive nuclear magnetic resonance (NMR) characterization complemented with other techniques (i.e. X-ray

diffraction, FTIR, EDS, elemental analysis, DLS, SEM) that helped to the assessment of the proper reaction conditions, and the chemical structure and properties of the particles. Finally, we evaluated the degradability of the particles and pH modifications after their immersion in physiological-like conditions.

2. EXPERIMENTAL SECTION

If not otherwise specified all reagent were purchased from Sigma-Aldrich.

2.1. Sol-gel precursors synthesis. P and Ca precursors were synthesized as previously published [22,24]. Briefly, phosphorus pentoxide ($\geq 99,99\%$) and metallic calcium granules PS (98%, Panreac) were oxidized in distilled absolute ethanol PRS (99,5%, Panreac) and anhydrous 2-methoxyethanol (99,8%) respectively by refluxing them at the solvent boiling point under Ar(g) atmosphere for 12 and 24 h respectively. We obtained 4 M ethylphosphate in ethanol and 1 M calcium 2-methoxyethoxide in 2-methoxyethanol. The solutions were filtered using 0.45 μm PTFE hydrophobic Minisart® SRP25 syringe filters (Sartorius AG, Göttingen, Germany) and stored under Ar(g) at $-20\text{ }^{\circ}\text{C}$.

2.2. CPG nanoparticles synthesis. Particles were synthesized by mixing different ratios (10:0, 8.5:1.5, 6:4, 1.5:8.5 and 0:10 mL) of the P and Ca precursors respectively in 90 mL of absolute ethanol (PRS, 99,5%, Panreac) (Tables 1a). Ammonia (PA-ACS, 30%, Panreac) was added dropwise under vigorous stirring until a suspension of particles was observed. After 12 h the particles were centrifuged, cleaned twice with absolute ethanol and once with hexane (ACS,

≈99%), and dried at 70 °C for 2 h. Dried particles were ground and stored in a desiccator under vacuum. For thermal treatment, particles were heated for 12 h at 200 or 350 °C in a muffle furnace L9/11 (Nabertherm, Lilienthal, Germany). Particles were weighted in a Sartorius CP224S analytical balance (Sartorius AG, Göttingen, Germany) to know yields and mass loss.

2.3. ¹H and ³¹P NMR spectroscopy. ¹H and ³¹P NMR analysis of the two precursors in anhydrous ethanol-d₆ (≈99,6%) and the dissolved particles (5 mg/mL) in D₂O (99.9%) plus 1.5% HCl (37%, Panreac) were performed using a Bruker 400 MHz Avance III spectrometer (Bruker, Billerica, MA, USA) equipped with a Prodigy TCI 5 mm cryoprobe. ¹H NMR conditions included; 3.66 μs pulse length, 30° tip angle, a recovery delay of 1 s, a total of 32 scans and an acquisition time of 2.5 s. Spectra were referenced to the ¹H nuclei of the deuterium solvent. ³¹P NMR conditions included; 3.76 μs pulse length, 30° tip angle, recovery delay of 1 s, a total of 256 scans and an acquisition time of 1.6 s. Spectrum were externally referenced to H₃PO₄ (85%) and ¹H nuclei was decoupled during ³¹P NMR spectrum acquisition. All spectrum were analyzed using the ACD/Spectrus Processor software (www.acdlabs.com).

2.4. Electrospray ionization mass spectrometry (ESI-MS). The Ca precursor was dissolved ~10⁴ times in absolute ethanol (PRS, 99.5%, Panreac) and analyzed on a ThermoFinnigan LTQ ion trap mass spectrometer (Thermo Fischer Scientific, Waltham, MA, USA). Instrument parameters included; sample infusion: 3 μL/min, spray voltage: 3.5 kV, capillary temperature: 200 °C, capillary voltage: 75 V, and tube lens voltage: 100 V. Mass spectra were acquired by the University of Kentucky Mass Spectrometry Facility.

2.5. Dynamic Light Scattering (DLS). The P and Ca precursors were dissolved separately and together in 1 mL of absolute ethanol (PRS, 99.5%, Panreac). The solutions were measured in a Zetasizer Nano ZS (Malvern, Worcestershire, UK) using a 10x2 mm precision Quartz Suprasil®

cell 115F-QS (Hellma®Analytics, Müllheim, Germany). Results were analyzed using the Zetasizer software version 7.12 (07/12/2016) (Malvern, Worcestershire, UK). Size population was expressed in volume percentage.

2.6. Particle composition and morphological images (EDS/FE-SEM). A Quanta Q200 scanning electron microscope (SEM) (FEI Company, Hillsboro, OR, USA) coupled with an energy dispersive X-ray spectroscopy detector (EDS) was used at 20.0 KV and 10 mm of working distance to quantify the approximate P and Ca atomic ratio of the particles. Values express the average of at least three different measurements. For morphological images, we used the NOVA NanoSEM-230 ultrahigh-resolution field emission scanning electron microscope (FE-SEM) (FEI Company, Hillsboro, OR, USA) at 5.00 KV and 5.0 mm working distance. In both cases, samples were coated with a thin carbon layer to improve conductivity. For morphological images, approximately 1 mg of the particles was dispersed in 1 mL of absolute ethanol PRS (99,5%, Panreac) and sonicated for several seconds. 2 μ L of the dispersion were added on silicon substrates and left to dry at room temperature.

2.7 Elemental analysis (EA). The samples were analyzed by combustion at 1060 °C in an elemental analyzer EA CE 1108 (Thermo Fischer Scientific, Waltham, MA, USA) to determine the C and N mass percentages. A mixture of vanadium pentoxide and lead powder was added to facilitate combustion, and atropine was used as a standard.

2.8. ^{31}P MAS NMR spectroscopy. ^{31}P MAS NMR spectra were acquired in a Bruker 400 MHz-WB Avance-II spectrometer (Bruker, Billerica, MA, USA), externally referenced to H_3PO_4 (85%). Approximately, 50 mg of the particles were placed in a ZrO_2 4mm rotor and spun at 12 kHz. Conditions include; 5 μ s pulse length, a 90° tip angle and 5 s of recovery delay. ^1H nuclei was decoupled using a Spinal-64 scheme at 73 watts power level.

2.9. X-ray diffraction (XRD). The particles were manually pressed in a cylindrical standard holder of 16x2.5 mm with the help of a glass plate. Samples were analyzed using a PANalytical X'Pert PRO MPD Alpha1 Powder Diffractometer (PANalytical, Almelo, Netherlands) in a Bragg-Brentano $\theta/2\theta$ geometry of 240 mm radius. The spectra were processed using the software ©PANalytical X'Pert HighScore (PANalytical, Almelo, the Netherlands) and the database PDF2 (2001) from the international center of diffraction data (ICDD).

2.10. Attenuated total reflectance infrared spectroscopy (ATR-FTIR). Approximately, 5 mg of the particles were analyzed in a Spectrum Two FT-IR Spectrometer (PerkinElmer, Waltham, MA, USA) coupled with an UATR Diamond/ZnSe accessory 1 reflection. Spectra were recorded between 4000 and 450 cm^{-1} with a resolution of 1 cm^{-1} . Spectra were processed using the software ©PerkinElmer Spectrum (PerkinElmer, Waltham, MA, USA) and the database ©2005-2008, Fiveash Data Management, Inc.

2.11. Degradability study of the CPG nanoparticles. Approximately, 3 mg of the particles ($n = 3$) were immersed in 1.3 mL of 0.05 M 4-(2-hydroxyethyl)piperazine-1-ethanesulfonic acid (HEPES) (99,5%) in miliQ water at $\text{pH}=7.4$. The resultant suspensions were incubated at 37 °C in a Memmert incubator (Memmert GmbH + Co KG, Schwabach, Germany). After 1 h and 1, 3, 6, 9, 14 days, particles were centrifuged and 1.1 mL of the media were extracted. Tubes were refilled with HEPES solution and incubated again at 37 °C. The extracted media were kept at -20 °C for further ion release and pH measurements.

2.12. Ion release measurements. The Ca^{2+} and inorganic phosphate (Pi) of the extracted solutions were measured by the O-Cresolphthalein complexone [26,27] and the Malachite green method [28], respectively. For the O-Cresolphthalein complexone, 4 μL of the extracted media were added onto 80 μL of 1.5 M 2-amino-2-methyl-1-propanol (AMP) ($\geq 90\%$) aqueous solution, maintaining

the pH at 10.4 by the addition of HCl (37%, Panreac). Then, 80 μ L of 0.16 mM O-Cresolphthalein, 6.8 mM 8-Hydroxyquinoline (99%) and 1.19 M HCl (37%, Panreac) aqueous solution were added. The reaction between the Ca^{2+} and the O-Cresolphthalein produce a purple complex that was measured by absorbance at 570 nm. A calibration curve (7.5, 5, 2, 1, 0.5, 0.1, 0 mM) of CaCl_2 ion solution for ion-selective electrodes (0.1 M) was prepared to convert absorbance to Ca^{2+} concentrations. The Pi content of the extracts was measured using the Phosphate Colorimetric Kit based on the Malachite green method [28]. A calibration curve of H_3PO_4 (25, 20, 15, 10, 5, 0 μ M) was prepared to convert absorbance to Pi concentrations. The absorbance was measured at 650 nm wavelength. All absorbance values were measured in an Infinite M200 Pro Microplate Reader (Tecan Group Ltd., Männedorf, Zürich, Switzerland).

2.13. pH measurements. The pH of each extraction was measured using a Crison 50 28 pH electrode and a Crison pH-Meter GLP 22+ (Hach Company, Loveland, CO, USA) previously calibrated with 4.01, 7.00 and 9.21 pH standard solutions.

2.14. Statistics. We used the GaphPad Prism 5 software to detect statistical significant differences in the ion release and pH measurements. We performed a two-way ANOVA grouped comparison analysis followed by a Bonferroni post-test to detect statistical significant differences between particles at each time point.

3. RESULTS AND DISCUSSION.

3.1. Sol-gel precursors characterization

We characterized the P and Ca precursors by NMR spectroscopy (Figure 1). Consistent with Ali et al. [29], we identified for the P precursor the formation of monoethylphosphate (MEP) and diethylphosphate (DEP) with traces of H_3PO_4 and triethylphosphate (TEP) (Figure 1a,b). Integrated intensities (Figure S1) justify the suggested peak assignment.

On the other hand, the fast exchangeable rate between the calcium 2-methoxyethoxide (CMEO) and the solvent 2-methoxyethanol (MEOH) of the Ca precursor led to an averaged signal for these two compounds (Figure 1c) [30], thus, hindering its characterization by NMR spectroscopy. However, the significant broad peaks in the spectrum indicate that a coordination of the MEO⁻ to a metallic center (i.e. Ca^{2+}) was occurring [31], which is consistent with the dark orange color observed for the Ca precursor (Figure S3), characteristic of electronic orbital transitions between metal ions and alkoxyalkoxide ligands [32–34]. In order to better elucidate the Ca precursor structure, we complemented the NMR characterization with mass spectrometry. Fortunately, ESI-MS analysis (Figure 1d) confirmed the formation of highly stable $[\text{Ca}(\text{MEOH})_3]^{2+}$ and $[\text{Ca}(\text{MEOH})_4]^{2+}$ metallic-coordinated complexes, which is consistent with the previous identification of hexa- and heptavalent calcium domains for the single crystal characterization of CMEO [35]. Note that Goel et al. [35] previously defined the formation of a larger cluster $[\text{Ca}_9(\text{MEO})_{18}(\text{MEOH})_2]$ than those observed in the ESI-MAS spectrum. However, we contemplate the possibility of the disruption of a bigger complex into smaller subunits during the ESI-MS analysis, since DLS measurements (Figure S2a) showed a significant large average cluster size of ~5 nm.

3.2. Interaction between the P and Ca precursors and precipitation of particles

There is a transition between the CMEO complex and the formation of a complex comprising Ca^{2+} and the hydroxyl groups (-OH) from the ethylphosphates as it was inferred after studying the interaction between the two precursors by NMR spectroscopy. We observed a peak broadening and shielding of the MEP and DEP signals when the two precursors were mixed together (P+Ca, [Figures 2a,b](#)). On the other hand, the peaks from the TEP remained unaltered and those from the CMEO shielded and became sharper ([Figure 2c](#)). All together indicates the disruption of the CMEO complex and the formation of a new one, comprising the Ca^{2+} and the hydroxyl groups of the ethylphosphates. DLS measurements ([Figure S2b](#)) supported this assumption, showing the disruption of the CMEO complex at ~ 5 nm and presenting a new one at ~ 1.8 nm. Interestingly, we observed a size increase of this new complex over time indicating that the sole interaction between the two precursors led to the spontaneous formation of particles or aggregates of ~ 1 μm after 30 h ([Figure S2c](#)). However, the addition of ammonia ($\text{NH}_{3(\text{aq})}$) catalyzed the formation and precipitation of particles by the induction of alkaline conditions. Since we decided to use $\text{NH}_{3(\text{aq})}$ to catalyze the reaction, we include the NMR characterization of the supernatant after the precipitation of particles. We observed the sole presence of DEP and TEP (P+Ca+ NH_3 , [Figures 2a,b](#)) in the supernatant, indicating that only the MEP and the small amount of H_3PO_4 precipitated with the Ca^{2+} ([Figure S4](#)). Notice that the absence of increase in the ethanol signal ([Figure 2a](#)) indicates the incorporation of the ethoxide groups into the particles.

3.3. Nanoparticle synthesis parameters

We studied different reaction parameters to obtain particles with different P/Ca ratios by combining different proportions of the two precursors in absolute ethanol under ammonia catalysis. The increase of P in the particle content followed an almost linear correlation with the

amount of P precursor used until the value reached a 55% (Tables 1a,b). Then, we needed significant high volumes of the P precursor to obtain compositions with $P > 55\%$. This is consistent with the previous detection of calcium MEP precipitation ($P+Ca+NH_3$, Figure 2a,b), which limited the P/Ca ratio of the particles to 1/1. The use of apolar solvents (e.g. 1,4-dioxane, toluene, hexane) could induce the precipitation of the highly ethanol-soluble calcium DEP and thus achieve particles with higher P contents. Focusing on the added $NH_{3(aq)}$ catalyst, we needed significant small amounts to synthesize P100, P65 and P55 particles, indicating different alkaline catalytic mechanisms of precipitation, i.e. while particles with high Ca contents needed high alkaline conditions, particles with higher P contents precipitated at more acidic conditions. In addition, we also included a preliminary morphological characterization of the particles (Figure S5). FE-SEM images showed the formation of aggregates ranging from several hundreds of nm to few μm , suggesting a high electrostatic interaction between smaller nanoparticles. Notice that after thermal treatment, we did not observe significant changes in particle morphology.

3.4. Characterization of the nanoparticles

At low temperatures, nanoparticles were mainly organically modified amorphous CPs. We characterized the chemical structure of the particles by ^{31}P MAS NMR and other complementary techniques. ^{31}P MAS NMR spectrum of the particles showed the presence of orthophosphate units (Q^0) (Figure 3a) [10] that together with the sole detection of P and Ca by EDS (Table 1a) and the absence of calcium phosphate (CP) crystalline structures (Figure 3c) [36–39], indicates the formation of amorphous CPs. We identified the formation of portlandite ($Ca(OH)_2$) and $NH_4H_2PO_4$ (Figure 3c,e) for the particles with a Ca excess (P30/P0) or its absence (P100) respectively, the Ca excess precipitated in form of $Ca(OH)_2$, and in its absence, the added $NH_{3(aq)}$ was incorporated as a

counter ion, this last is consistent with the significant N amount detected by EA for P100 particles (Table 1b). Notice that the absence of N in the rest of compositions excludes the formation of ammonium salts for the other particles. In order to identify the presence of organics, we characterized by ^1H NMR the dissolution of the particles in acidic D_2O (Figure 4a). The spectrum analysis confirmed the presence of one majoritarian ethylphosphate, assigned to the precipitation of calcium MEP (CMEP) based on the previous NMR characterization (Figures 2a) that showed the only incorporation of MEP into the particles. The increased amount of C with the P content, detected by EA (Table 1b), is consistent with the precipitation of CMEP. These results complements previous studies, in which we developed similar particles doped with small amounts of Ti^{4+} and Na^+ for angiogenic and osteogenic purposes [22,24,40]. In such studies, we described the presence of organics in the particles but not much information was given about its chemical structure. The results clarify that after synthesis the particles are amorphous calcium orthophosphates containing ethoxide groups (i.e. CMEP) rather than inorganic CPGs. We also complemented the characterization of the particles by ATR-FTIR spectroscopy (Figure 3e), the spectrum exhibited extra vibrational bands, apart from those assigned to inorganic CPs (i.e. $\nu_4(\text{OPO})$, $\nu_1(\text{PO})$ and $\nu_3(\text{PO})$ [36,37,41]), assigned to the vibration of the ethoxide groups (e.g. $\nu_s(\text{CCO})$ and $\nu_{as}(\text{CCO})$ [38,42,43]). A curious observation is the sharp ATR-FTIR and ^{31}P MAS NMR peaks (Figure 3a,e) typically observed in well-ordered crystalline structures due to intrinsic high atomic mobility. However, the absence of crystalline CPs in the XRD spectrum (Figure 3c), suggests that the presence of ethoxide groups disrupted the crystalline lattice but still allow a high atomic mobility. Indeed, the leftmost peak in the XRD spectra (marked with a star) might be assigned to some diffraction plane of the CMEP. On the contrary, P55 particles exhibited wider peaks (Figure 3a,e), indicating a higher connectivity.

3.5. Thermally treated particles

For thermally treated nanoparticles, the higher the P content the higher the glassy structure. In order to stabilize the chemical structure of the particles and eliminate organics with a possible undesired cytotoxicity, we hold nanoparticles to a thermal treatment at 200 or 350 °C. Particles were characterized using the same previous techniques. After thermal treatment, we observed an increase in the phosphate condensation (Q^2 and Q^1 units) (Figure 3b) [38,43]. The lack of phosphate condensation in alkaline and acidic conditions during synthesis (Figure 3a, Figure 4a) indicates that phosphate condensation is only catalyzed at temperatures around 200 °C, as it has been reported in previous studies [20,43,44]. On the other hand, the P100 particles decomposed probably to $NH_{3(g)}$ and $H_3PO_{4(l)}$ after thermal treatment. At the same time, we observed the almost total elimination of the C content (Table 1c), indicating the decomposition of the ethoxide groups. Notice that the C content for P30-350°C and P0-350°C particles (Table 1c) is attributed to the carbonation of the portlandite to calcite at a minimum temperature of 350°C (Figure 3d,f), in fact, this is consistent with the significant mass increase of P0-350°C particles while the other compositions significantly reduced its weight due to the elimination of ethoxides (Table 1a). The 1H NMR characterization of the dissolved particles in acidic D_2O (Figure S7) confirmed the elimination of ethoxides, except for a tiny amount in P65-200°C. Paying attention to the XRD characterization (Figure 3d), we observed an amorphous-like structure for the CPs after thermal treatment, which is confirmed by the broad peaks observed in the ^{31}P MAS NMR and ATR-FTIR spectra (Figure 3d,f) [38,43,45]. Considering that phosphate condensation and amorphicity occurred, we can confirm that after a thermal treatment at 200 °C the particles made a transition to a more glassy structure as higher was their P content. In fact, the ATR-FTIR spectrum showed the typical bands of CPGs [38,43] and amorphous-like CPs (ACPs) [41] (e.g. $\delta(POP)$, $\nu_{as}(POP)$, $\nu_{as}(PO_3^{2-})$ and $\nu_{as}(PO_2^-)$), and additionally the ethoxide bands were not observed any more,

confirming their decomposition [42]. In parallel, we identified by ^{31}P NMR the different Q^n units when the particles were dissolved in acidic D_2O (Figure 4b), which indicates the release of ortho/pyro and metaphosphate units after the degradation of the particles. Since the resolution of the ^{31}P NMR spectrum (Figure 4b) was higher than in the ^{31}P MAS NMR, we used the relative abundance of the Q^n units from the ^{31}P NMR spectra (Table S4) to quantify the different phosphate units. We assigned the Q^2 units to cyclic or open chained amorphous calcium trimetaphosphate (ACTMP), the Q^1 units to open chained ACTMP or amorphous calcium pyrophosphate (ACPP) and the Q^0 units to amorphous calcium orthophosphate (ACP) [18,45,46]. We did not consider the formation of longer metaphosphates due to the high amount of Q^1 units. On the other hand, the ratio $Q^2:Q^1 > 1:2$ for P65-200°C indicates the formation of cyclic ACTMP or longer metaphosphates.

To the best of our knowledge, this is the first time that binary CPGs [20,38,43] or ACPs [39,41,45] nanoparticles are synthesized by the sol-gel method using metal alkoxides. We only found a study of binary micrometric CPGs synthesized by melt-quenching [18]. In that study, Fletcher et al. [18] synthesized CPGs with lower Ca contents and they observed the formation of crystalline pyrophosphates when $\text{CaO}:\text{P}_2\text{O}_5 \geq 1.21$. As mentioned, the synthesis of binary CPGs is of interest for a straightforward synthesis and higher biocompatibility. If we compare our glasses with conventional CPGs, we observe a lower degree of phosphate condensation [18,21,43], which is assigned to the higher content of Ca^{2+} , and inevitably disrupted the P_2O_5 network. Since the current characterization of CPGs with high Ca^{2+} contents remains poorly understood [10], we consider that the information presented in this study is relevant for the materials science community.

3.6. Ion release and pH modifications of the CPGs nanoparticles in physiological conditions

Middle compositions are more likely to be applied in terms of degradation. The last part of this study consisted on the evaluation of the ion release and pH modification after the immersion of the particles in 0.05 M HEPES buffered medium at physiological-like conditions (i.e. pH 7.4 and 37 °C). Before thermal treatments, the particles were very soluble (Figure 5a), releasing high amounts of Ca^{2+} in short periods. We assigned the high solubility of the particles to the presence of ethoxides, which likely disrupts the CP chemical lattice making it less stable. The low inorganic phosphate (Pi) release (Figure 5c), except for P100 that was mainly inorganic $\text{NH}_4\text{H}_2\text{PO}_4$, is attributed to the release of MEP instead. The Malachite green method used is selective of free inorganic phosphate and may be unsuitable for the detection of organophosphate compounds [28]. Moreover, we know of the release of MEP in strong acidic conditions by the previous ^1H NMR characterization (Figure 4a). If we compare our organically modified particles at low temperature with conventional inorganic CPGs [11,47,48] or ACPs [49,50], the Ca^{2+} release was significant faster, indicating a potential applicability where high initial Ca^{2+} concentrations are needed (e.g. chemotaxis, angiogenesis, osteogenesis, wound healing, etc.) [5,22,40,51]. However, the strong basification induced by the dissolution of high amounts of portlandite by the P0 particles (Figure 5e) may limit their use for biological applications. In regards of cytotoxicity, we consider important to study the metabolization of the released MEP due to their high stability (Figure 4a), although similar particles did not show cytotoxicity in previous studies [22,40]. Finally, P100 particles may be interesting to increase the Pi concentration without pH modifications (Figure 5e) but considering the effects of simultaneously releasing high amounts of NH_4^+ .

After thermal treatment, the degradability of the particles was more sustained (Figure 5b,d), releasing Ca^{2+} and Pi up to two weeks without significant pH modifications (Figure 5f). Notice that after thermal treatment the Pi release was higher due to the conversion of the MEP to Pi. We attribute the higher stability of the particles to a higher degree of calcium-phosphate interactions,

phosphate condensation and elimination of ethoxides. We would like to highlight that even though the release of pyrophosphates is thought to contribute in bone mineralization [52], the stability of higher condensed phosphate units (i.e. trimetaphosphates) under strong acidic conditions (Figure 4b) justifies further studies of how these molecules are metabolized in the body. Correlating these results with the previous particle characterization, we identified that the particles containing ACTMP, are more suitable to release sustained higher amounts of Pi, while the ones containing ACP would be ideal for modulating higher bioactive Ca^{2+} concentration releases. Although P0-350°C showed the highest Ca^{2+} release, Denoux et al. [53] previously reported the insolubility of CaCO_3 in cell culture conditions, probably due to the $\text{CO}_{2(\text{g})}/\text{HCO}_{3-(\text{liq.})}$ buffer equilibrium of conventional incubators. Nevertheless, many reports have shown the resorption of CaCO_3 *in vivo* [54,55], which suggests that the P0-350°C particles would be suitable as a biological Ca^{2+} source. In comparison to reported multicomponent CPG systems [11,47,48] or conventional coprecipitated ACPs [49,50], the ion release rate of the thermally treated particles in this study was similar or even higher, suggesting their applicability in similar biomedical purposes (i.e. bone regeneration, angiogenesis, wound healing, etc.). Notice that the still high amount of particles after the degradability assay (Figure S8) suggests that further ion release could continue at longer times. We would like to remark the importance of initial increases in the extracellular Ca^{2+} concentrations. Our group has previously described and evidenced a proposed angiogenic mechanism involving cell membrane Ca^{2+} -sensing receptors, in which it seems that Ca^{2+} ions, apart from participate in osteogenesis, cell chemotaxis and other favorable metabolic responses, play a pivotal role in the stimulation of initial vasculature formation [56]. This can lead to the restoration of impaired wound healing in other tissues apart from bone as our group has recently shown for skin wound healing applications [51,57]. We have focused the current study in the in-depth structural characterization of binary CPGs with high Ca^{2+} contents but further structural and biological studies should be

perform with these new designed nanoparticles in combination with supporting biodegradable biomaterials in order to build 3D architectures for tissue regeneration.

4. CONCLUSIONS

In summary, the study of novel binary (P_2O_5 -CaO) CPGs with high CaO contents synthesized by the sol-gel method is of interest due to a straightforward synthesis, lack of unknown metabolizable ions and increase of bioactive Ca^{2+} release. Since the synthesis of CPGs with high CaO contents remains uncertain, this study is relevant for the material science community. At the same time, we also shed light on the chemical structure and reactivity of novel sol-gel precursors (i.e. ethylphosphate and calcium 2-methoxyethoxide) that are becoming increasingly relevant for the polycondensation of metal oxides to gradually substitute current developed CPGs participating in really sophisticated architecture but with unsuitable or poor controlled bioactive ion releases.

ASSOCIATED SUPPLEMENTARY MATERIAL

NMR integrated intensities, relative abundances and peak assignments, DLS measurements, Ca precursor color image, FE-SEM images, ATR-FTIR band assignments and comparison with standard database, image of the particles after the degradability assay, statistics.

AUTHOR INFORMATION

Corresponding Author

*E-mail: oscar.castano@ub.edu, eengel@ibebarcelona.eu

DISCLOSURE

The authors declare no competing financial interest.

ACKNOWLEDGMENTS

We thank Dr. Joan Pous from the Structural & Computational Biology Unit at the Institute for Research in Biomedicine (IRB), 08028 Barcelona, Spain for allowing us to use the DLS equipment.

FUNDING

The authors thank the Spanish Ministry-MINECO (MAT2011-29778-C02-01), the European Commission-ERANET (nAngiofrac PI11/03030), Obra Social la Caixa (CaixaImpulse CI0015) and the Serra Hunter program for funding.

ABBREVIATIONS

BC, bioactive ceramic; BGs, bioactive glass; CP, calcium phosphate; CPG, calcium phosphate glass; MEP, monoethylphosphate; DEP, diethylphosphate; TEP, triethylphosphate; CMEO, calcium 2-methoxyethoxide; MEOH, 2-methoxyethanol; CMEP, calcium monoethylphosphate; CDEP, calcium diethylphosphate; ACP, amorphous calcium phosphate; ACP, amorphous calcium pyrophosphate; ACTMP, amorphous calcium trimetaphosphate; Pi, inorganic phosphate.

REFERENCES

- [1] A. Malhotra, P. Habibovic, Calcium Phosphates and Angiogenesis: Implications and Advances for Bone Regeneration, *Trends Biotechnol.* 34 (2016) 983–992. doi:10.1016/j.tibtech.2016.07.005.

- [2] D.H. Bach, H.J. Park, S.K. Lee, The Dual Role of Bone Morphogenetic Proteins in Cancer, *Mol. Ther. - Oncolytics*. 8 (2018) 1–13. doi:10.1016/j.omto.2017.10.002.
- [3] E.L. Lord, J.R. Cohen, Z. Buser, H.J. Meisel, D.S. Brodke, S.T. Yoon, J.A. Youssef, J.C. Wang, J.B. Park, Trends, Costs, and Complications of Anterior Cervical Discectomy and Fusion With and Without Bone Morphogenetic Protein in the United States Medicare Population, *Glob. Spine J.* 7 (2017) 603–608. doi:10.1177/2192568217699207.
- [4] S. Kargozar, F. Baino, S. Hamzehlou, R.G. Hill, M. Mozafari, Bioactive Glasses: Sprouting Angiogenesis in Tissue Engineering, *Trends Biotechnol.* 36 (2018) 430–444. doi:10.1016/j.tibtech.2017.12.003.
- [5] a Aguirre, a González, J. a Planell, E. Engel, Extracellular calcium modulates in vitro bone marrow-derived Flk-1+ CD34+ progenitor cell chemotaxis and differentiation through a calcium-sensing receptor., *Biochem. Biophys. Res. Commun.* 393 (2010) 156–61. doi:10.1016/j.bbrc.2010.01.109.
- [6] S.P. Valappil, J.C. Knowles, M. Wilson, Effect of silver-doped phosphate-based glasses on bacterial biofilm growth, *Appl. Environ. Microbiol.* 74 (2008) 5228–5230. doi:10.1128/AEM.00086-08.
- [7] A. Wajda, W.H. Goldmann, R. Detsch, A.R. Boccaccini, M. Sitarz, Influence of zinc ions on structure, bioactivity, biocompatibility and antibacterial potential of melt-derived and gel-derived glasses from CaO-SiO₂ system, *J. Non. Cryst. Solids*. 511 (2019) 86–99. doi:10.1016/j.jnoncrysol.2018.12.040.
- [8] FDA, Guidance for Industry Class II Special Controls Guidance Document : Resorbable Calcium Salt Bone Void Filler Device ; Guidance for Industry and FDA Staff,

- Management. 510 (2003) 1–10.
- [9] A.R. Jones, R. Winter, G.N. Greaves, I.H. Smith, MAS NMR study of soda-lime-silicate glasses with variable degree of polymerisation, *J. Non. Cryst. Solids*. 293–295 (2001) 87–92. doi:10.1016/S0022-3093(01)00656-1.
- [10] J.C. Knowles, Phosphate based glasses for biomedical applications, *J. Mater. Chem.* 13 (2003) 2395–2401. <http://dx.doi.org/10.1039/B307119G>.
- [11] M. Navarro, M. Ginebra, J. Clément, S. Martinez, G. Avila, J.A. Planell, Physicochemical degradation of titania-stabilized soluble phosphate glasses for medical applications, *J. Am. Ceram. Soc.* 86 (2003) 1342–52.
- [12] J. V. Rau, M. Curcio, M.G. Raucchi, K. Barbaro, I. Fasolino, R. Teghil, L. Ambrosio, A. De Bonis, A.R. Boccaccini, Cu-Releasing Bioactive Glass Coatings and Their in Vitro Properties, *ACS Appl. Mater. Interfaces*. 11 (2019) 5812–5820. doi:10.1021/acsami.8b19082.
- [13] B. Daley, A.T. Doherty, B. Fairman, C.P. Case, Wear debris from hip or knee replacements causes chromosomal damage in human cells in tissue culture., *J. Bone Joint Surg. Br.* 86 (2004) 598–606. doi:10.1302/0301-620X.86B4.14368.
- [14] A.C. Cheung, S. Banerjee, J.J. Cherian, F. Wong, J. Butany, C. Gilbert, C. Overgaard, K. Syed, M.G. Zywiell, J.J. Jacobs, M.A. Mont, Systemic cobalt toxicity from total hip arthroplasties: review of a rare condition Part 1 - history, mechanism, measurements, and pathophysiology, *Bone Joint J.* 98-B (2016) 6–13. doi:10.1302/0301-620X.98B1.36374.
- [15] S.A. Lowndes, A.L. Harris, The role of copper in tumour angiogenesis, *J. Mammary Gland Biol. Neoplasia*. 10 (2005) 299–310. doi:10.1007/s10911-006-9003-7.

- [16] J.R. Jones, Review of bioactive glass : From Hench to hybrids, *Acta Biomater.* 23 (2015) S53–S82. doi:10.1016/j.actbio.2015.07.005.
- [17] V. Salih, K. Franks, M. James, G.W. Hastings, J.C. Knowles, I. Olsen, Development of soluble glasses for biomedical use Part II: The biological response of human osteoblast cell lines to phosphate-based soluble glasses, *J. Mater. Sci. Mater. Med.* 11 (2000) 615–620. doi:10.1023/A:1008901612674.
- [18] J.P. Fletcher, R.J. Kirkpatrick, D. Howell, S.H. Risbud, 31P Magic-angle Spinning Nuclear Magnetic Resonance Spectroscopy of Calcium Phosphate Glasses, *J. Chem. Soc. Faraday Trans.* 89 (1993) 3297–3299.
- [19] C. Peticone, D.D.S. Thompson, G.J. Owens, H. Kim, M. Micheletti, J.C. Knowles, I. Wall, Towards modular bone tissue engineering using Ti – Co-doped phosphate glass microspheres : cytocompatibility and dynamic culture studies, *J. Biomater. Appl.* 32 (2017) 295–310. doi:10.1177/0885328217720812.
- [20] D.M. Pickup, S.P. Valappil, R.M. Moss, H.L. Twyman, P. Guerry, M.E. Smith, M. Wilson, J.C. Knowles, R.J. Newport, Preparation, structural characterisation and antibacterial properties of Ga-doped sol–gel phosphate-based glass, *J. Mater. Sci.* 44 (2009) 1858–1867. doi:10.1007/s10853-008-3237-2.
- [21] D. Carta, D.M. Pickup, J.C. Knowles, I. Ahmed, M.E. Smith, R.J. Newport, A structural study of sol–gel and melt-quenched phosphate-based glasses, *J. Non. Cryst. Solids.* 353 (2007) 1759–1765. doi:10.1016/j.jnoncrysol.2007.02.008.
- [22] H. Oliveira, S. Catros, C. Boiziau, R. Siadous, J. Marti-Munoz, R. Bareille, S. Rey, O. Castano, J. Planell, J. Amédée, E. Engel, The proangiogenic potential of a novel calcium

- releasing biomaterial: Impact on cell recruitment., *Acta Biomater.* 29 (2016) 435–45. doi:10.1016/j.actbio.2015.10.003.
- [23] A.R. Romero, N. Toniolo, A.R. Boccaccini, E. Bernardo, Glass-ceramic foams from “weak alkali activation” and gel-casting of waste glass/fly ash mixtures, *Materials (Basel)*. 12 (2019) 1–14. doi:10.3390/ma12040588.
- [24] N. Sachot, O. Castaño, H. Oliveira, J. Martí-Muñoz, A. Roguska, J. Amedee, M. Lewandowska, J.A. Planell, E. Engel, A novel hybrid nanofibrous strategy to target progenitor cells for cost-effective in situ angiogenesis, *J. Mater. Chem. B*. 4 (2016) 6967–6978. doi:10.1039/C6TB02162J.
- [25] B. Yu, C.A. Turdean-Ionescu, R.A. Martin, R.J. Newport, J. V Hanna, M.E. Smith, J.R. Jones, Effect of Calcium Source on Structure and Properties of Sol–Gel Derived Bioactive Glasses, *Langmuir*. 28 (2012) 17465–17476. doi:10.1021/la303768b.
- [26] H.J. Gitelman, An improved automated procedure for the determination of calcium in biological specimens, *Anal. Biochem.* 18 (1967) 521–531.
- [27] E. Gindler, J. King, Rapid colorimetric determination of calcium in biologic fluids with methylthymol blue ., *Am. J. Clin. Pathol.* 58 (1972) 376–382.
- [28] S.G. Carter, D.W. Karl, Inorganic phosphate assay with malachite green: An improvement and evaluation, *J. Biochem. Biophys. Methods*. 7 (1982) 7–13. doi:10.1016/0165-022X(82)90031-8.
- [29] A.F. Ali, P. Mustarelli, E. Quartarone, A. Magistris, Improving the synthesis of alkyl phosphates a sol-gel precursors, *J. Mater. Res.* 14 (1999) 327–329.

- [30] R.R. Biekofsky, S.R. Martin, J.P. Browne, P.M. Bayley, J. Feeney, Ca²⁺ Coordination to Backbone Carbonyl Oxygen Atoms in Calmodulin and Other EF-Hand Proteins : ¹⁵N Chemical Shifts as Probes for Monitoring Individual-Site Ca²⁺ Coordination†, *Biochemistry*. 37 (1998) 7617–7629. doi:10.1021/bi9800449.
- [31] V. Peruzzo, M. Andrea Chiurato, P. Tomasin, N. Brianese, P. Traldi, M. Favaro, Study of challenging calcium alkoxides in solution by electrospray ionisation mass spectrometry (Part 2), *Eur. J. Mass Spectrom.* 19 (2013) 453–461. doi:10.1255/ejms.1253.
- [32] E.C. Hayes, T.R. Porter, C.J. Barrows, W. Kaminsky, J.M. Mayer, S. Stoll, Electronic Structure of a CuII-Alkoxide Complex Modeling Intermediates in Copper-Catalyzed Alcohol Oxidations, *J. Am. Chem. Soc.* 138 (2016) 4132–4145. doi:10.1021/jacs.5b13088.
- [33] K.L. Taft, A. Caneschi, L.E. Pence, C.D. Delfs, G.C. Papaefthymiou, S.J. Lippard, Iron and Manganese Alkoxide Cubes, *J. Am. Chem. Soc.* 115 (1993) 11753–11766. doi:10.1021/ja00078a014.
- [34] C. Kleinlein, S.L. Zheng, T.A. Betley, Ground State and Excited State Tuning in Ferric Dipyrrin Complexes Promoted by Ancillary Ligand Exchange, *Inorg. Chem.* 56 (2017) 5892–5901. doi:10.1021/acs.inorgchem.7b00525.
- [35] S.C. Goel, M.A. Matchett, M.Y. Chiang, W.E. Buhro, A Very Large Calcium Dialkoxide Molecular Aggregate Having a CdI₂Core Geometry: Ca₉(OCH₂CH₂OMe)₁₈(HOCH₂CH₂OMe)₂, *J. Am. Chem. Soc.* 113 (1991) 1844–1845. doi:10.1021/ja00005a066.
- [36] A. Taha, M. Akram, Z. Jawad, A.Z. Alshemary, R. Hussain, Strontium doped injectable bone cement for potential drug delivery applications, *Mater. Sci. Eng. C*. 80 (2017) 93–101.

- doi:10.1016/j.msec.2017.05.117.
- [37] A. Paz, D. Guadarrama, M. López, J.E. González, N. Brizuela, J. Aragón, A comparative study of hydroxyapatite nanoparticles synthesized by different routes, *Quim. Nov.* 35 (2012) 1724–1727.
- [38] D. Carta, J.C. Knowles, M.E. Smith, R.J. Newport, Synthesis and structural characterization of P2O5–CaO–Na2O sol–gel materials, *J. Non. Cryst. Solids.* 353 (2007) 1141–1149. <http://www.sciencedirect.com/science/article/pii/S0022309306013445>.
- [39] T. Windarti, Taslimah, A. Haris, Y. Astuti, A. Darmawan, Synthesis of β -Calcium Pyrophosphate by sol-gel method, *IOP Conf. Ser. Mater. Sci. Eng.* 172 (2017) 012058. doi:10.1088/1757-899X/172/1/012058.
- [40] H. Oliveira, S. Catros, O. Castano, S. Rey, R. Siadous, D. Clift, J. Marti-Munoz, M. Batista, R. Bareille, J. Planell, E. Engel, J. Amédée, The proangiogenic potential of a novel calcium releasing composite biomaterial: Orthotopic in vivo evaluation, *Acta Biomater.* (2017). doi:<http://doi.org/10.1016/j.actbio.2017.02.039>.
- [41] L. Jiang, Y. Li, Y. Shao, Y. Zhang, R. Han, S. Li, W. Wai, Enhanced removal of humic acid from aqueous solution by novel stabilized nano-amorphous calcium phosphate : Behaviors and mechanisms, *Appl. Surf. Sci.* 427 (2018) 965–975. doi:10.1016/j.apsusc.2017.08.104.
- [42] B.C. Smith, The C-O, Bond Part I : Introduction and the Infrared Spectra of Alcohols, *Spectroscopy.* 32 (2017) 14–21.
- [43] D.M. Pickup, P. Guerry, R.M. Moss, J.C. Knowles, M.E. Smith, R.J. Newport, New sol–gel synthesis of a (CaO)0.3(Na2O)0.2(P2O5)0.5 bioresorbable glass and its structural characterisation, *J. Mater. Chem.* 17 (2007) 4777–4784. doi:10.1039/b709955j.

- [44] H.-W. Kim, O. Vermesh, F. Foroutan, S.S. Gambhir, J.C. Knowles, J. V. Jokerst, Sol–Gel Synthesis and Electrospinning of Biodegradable $(\text{P}_2\text{O}_5)_{55}-(\text{CaO})_{30}-(\text{Na}_2\text{O})_{15}$ Glass Nanospheres as a Transient Contrast Agent for Ultrasound Stem Cell Imaging, *ACS Nano*. 9 (2015) 1868–1877. doi:10.1021/nm506789y.
- [45] R. Mathew, P.N. Gunawidjaja, I. Izquierdo-Barba, K. Jansson, A. García, D. Arcos, M. Vallet-Regí, M. Edén, Solid-State ^{31}P and ^1H NMR Investigations of Amorphous and Crystalline Calcium Phosphates Grown Biomimetically From a Mesoporous Bioactive Glass, *J. Phys. Chem. C*. 115 (2011) 20572–20582. doi:10.1021/jp206237n.
- [46] I. Abrahams, K. Franks, G.E. Hawkes, G. Philippou, J. Knowles, T. Nunes, ^{23}Na , ^{27}Al and ^{31}P NMR and X-ray powder diffraction study of Na/Ca/Al phosphate glasses and ceramics, *J. Mater. Chem.* 7 (1997) 1573–1580.
- [47] J.C. Knowles, K. Franks, I. Abrahams, Investigation of the solubility and ion release in the glass system $\text{K}_2\text{O}-\text{Na}_2\text{O}-\text{CaO}-\text{P}_2\text{O}_5$, *Biomaterials*. 22 (2001) 3091–3096.
- [48] I. Ahmed, M. Lewis, I. Olsen, J.C. Knowles, Phosphate glasses for tissue engineering : Part 1 . Processing and characterisation of a ternary-based $\text{P}_2\text{O}_5-\text{Ca}-\text{Na}_2\text{O}$ glass system, *Biomaterials*. 25 (2004) 491–499. doi:10.1016/S0142-9612(03)00546-5.
- [49] M.A.S. Melo, M.D. Weir, V.F. Passos, M. Powers, H.H.K. Xu, Ph-activated nano-amorphous calcium phosphate-based cement to reduce dental enamel demineralization, *Artif. Cells, Nanomedicine Biotechnol.* 45 (2017) 1778–1785. doi:10.1080/21691401.2017.1290644.
- [50] M. Yang, J. Ren, R. Zhang, Novel gallium-doped amorphous calcium phosphate nanoparticles: Preparation, application and structure study, *J. Non. Cryst. Solids*. 466–467

- (2017) 15–20. doi:10.1016/j.jnoncrysol.2017.03.034.
- [51] C. Navarro-Requena, J.D. Weaver, A.Y. Clark, D.A. Clift, S. Pérez-Amodio, Ó. Castaño, D.W. Zhou, A.J. García, E. Engel, PEG hydrogel containing calcium-releasing particles and mesenchymal stromal cells promote vessel maturation, *Acta Biomater.* (2017). doi:10.1016/j.actbio.2017.12.009.
- [52] Z. Zyman, A. Goncharenko, D. Rokhmistrov, Kinetics and mechanisms of the transformation of precipitated amorphous calcium phosphate with a Ca/P ratio of 1:1 to calcium pyrophosphates, *J. Cryst. Growth.* 478 (2017) 117–122. doi:10.1016/j.jcrysgro.2017.08.031.
- [53] C.B.S.S. Danoux, D.C. Bassett, Z. Othman, A.I. Rodrigues, R.L. Reis, J.E. Barralet, C. a. van Blitterswijk, P. Habibovic, Elucidating the individual effects of calcium and phosphate ions on hMSCs by using composite materials, *Acta Biomater.* 17 (2015) 1–15. doi:10.1016/j.actbio.2015.02.003.
- [54] A. Som, R. Raliya, L. Tian, W. Akers, J.E. Ippolito, S. Singamaneni, P. Biswas, S. Achilefu, Monodispersed calcium carbonate nanoparticles modulate local pH and inhibit tumor growth: In vivo, *Nanoscale.* 8 (2016) 12639–12647. doi:10.1039/c5nr06162h.
- [55] E.A. Genina, Y.I. Svenskaya, I.Y. Yanina, L.E. Dolotov, N.A. Navolokin, A.N. Bashkatov, G.S. Terentyuk, A.B. Bucharskaya, G.N. Maslyakova, D.A. Gorin, V. V. Tuchin, G.B. Sukhorukov, In vivo optical monitoring of transcutaneous delivery of calcium carbonate microcontainers, *Biomed. Opt. Express.* 7 (2016) 2082. doi:10.1364/boe.7.002082.
- [56] A. Aguirre, A. González, M. Navarro, O. Castaño, J.A. Planell, E. Engel, Control of microenvironmental cues with a smart biomaterial composite promotes endothelial

progenitor cell angiogenesis, *Eur. Cells Mater.* 24 (2012) 90–106.

- [57] C. Navarro-Requena, S. Pérez-Amodio, O. Castano, E. Engel, Wound healing-promoting effects stimulated by extracellular calcium and calcium-releasing nanoparticles on dermal fibroblasts, *Nanotechnology.* 29 (2018). doi:10.1088/1361-6528/aad01f.

DATA AVAILABILITY

The raw data required to reproduce these findings are available to download from <https://tinyurl.com/y74gp8do>.

ACCEPTED MANUSCRIPT

Scheme captions:

Scheme 1. Mono/di/triethylphosphate (MEP/DEP/TEP) and calcium 2-methoxyethoxide (CMEO) proposed chemical structures.

Table captions

Table 1. Particle synthesis conditions, yields and mass loss **a)**. Particle composition before **b)** and after thermal treatment **c)**. P/Ca atomic % were measured by EDS and C and N mass % by EA.

ACCEPTED MANUSCRIPT

Figures captions:

Figure 1. ^1H NMR **a)** and ^{31}P NMR **b)** spectra of the P precursor in ethanol- d_6 . Integrated intensities and relative abundance in [Figure S1](#) and [Table S1](#). Notice that the EtOH of the P precursor was removed by evaporation. ^1H NMR **c)** and ESI-MS spectra **d)** of the Ca precursor.

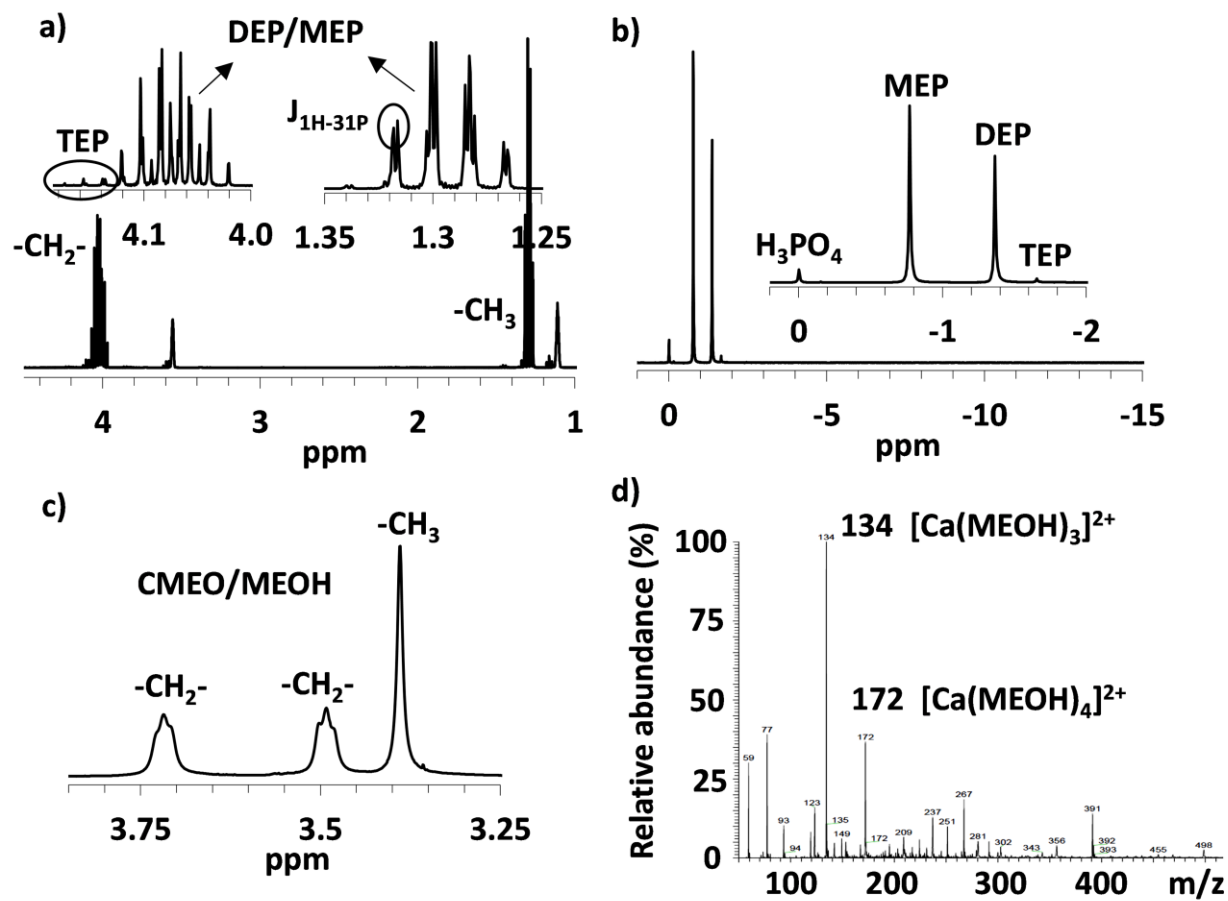
Figure 2. ^1H NMR **a)** and ^{31}P NMR **b)** spectra of the P precursor (P), the P precursor after the addition of Ca precursor (P+Ca) and the supernatant after the precipitation of particles by the addition of ammonia (P+Ca+ NH_3). For full spectra and integrated intensities please refer to [Figure S4](#). ^1H NMR spectra of the Ca precursor before and after the addition of the P precursor **c)**. Notice that in **c)** the P precursor was not purified and contained EtOH. Ca precursor was added in excess until we did not observe further changes in the spectrum. $\text{NH}_{3(\text{aq})}$ was added until a precipitation of particles was observed.

Figure 3. ^{31}P MAS NMR, XRD and ATR-FTIR spectra of the particles before **a,c,e)** and after thermal treatment **b,d,f)**. ^{31}P MAS NMR chemical shifts and relative abundances in [Table S2](#). ATR-FTIR band assignment in [Table S3](#).

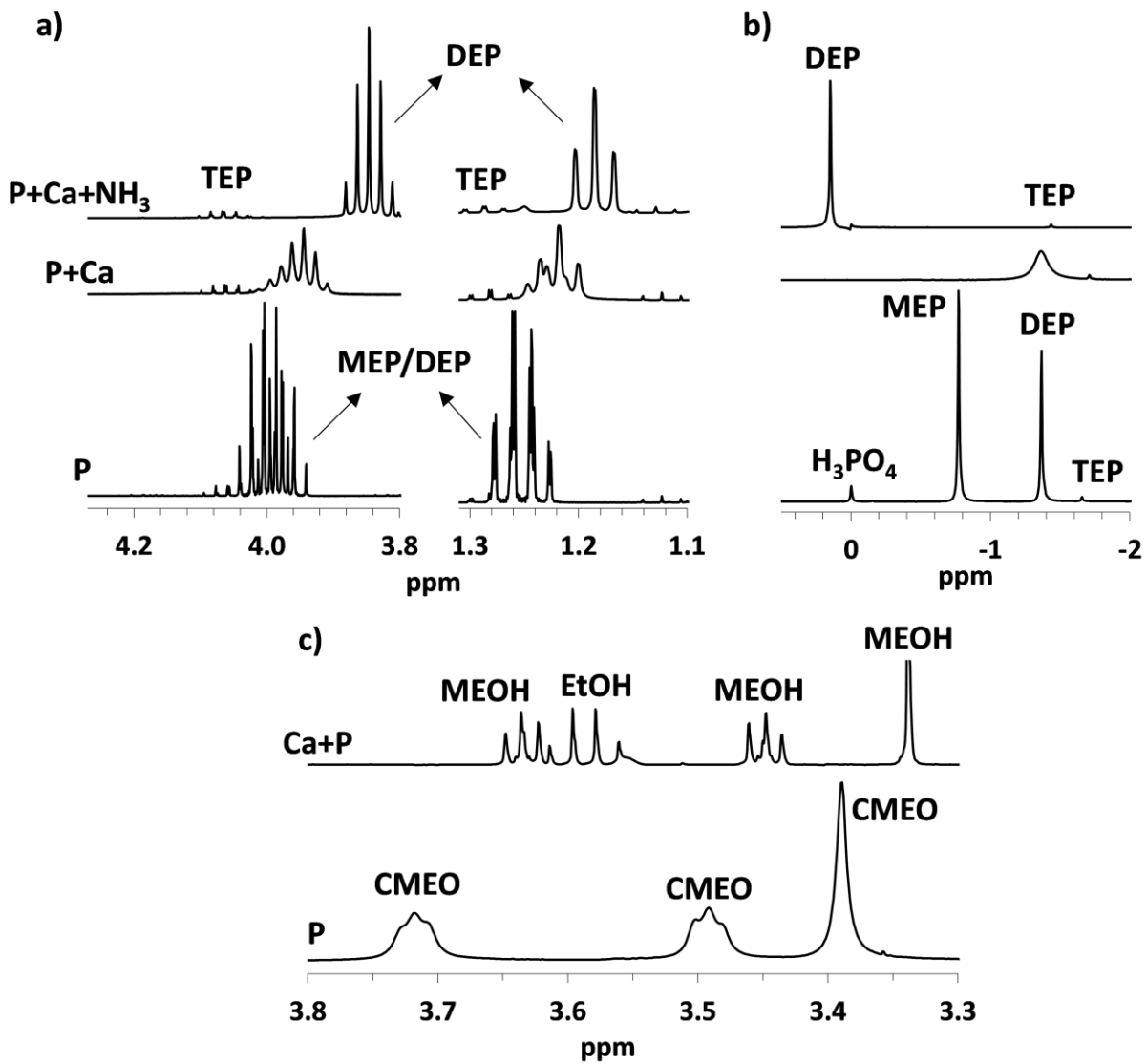
Figure 4. ^1H NMR spectra of the dissolved particles before thermal treatment in acidic D_2O **a)**. Notice that the acetone in P0-RT is assigned to impurities from NMR tube cleaning. ^{31}P NMR spectra of the dissolved particles after thermal treatment **b)**. Chemical shift and relative abundance in [Table S4](#).

Figure 5. Ca^{2+} , Pi and pH modifications after the immersion of the particles in 0.05 M HEPES solution at pH 7.4 and 37 °C before **a,c,e)** and after thermal treatment **b,d,f)**. Media were replaced every time point. Values represent means and error bars standard deviation. Statistical analysis in [Table S5](#).

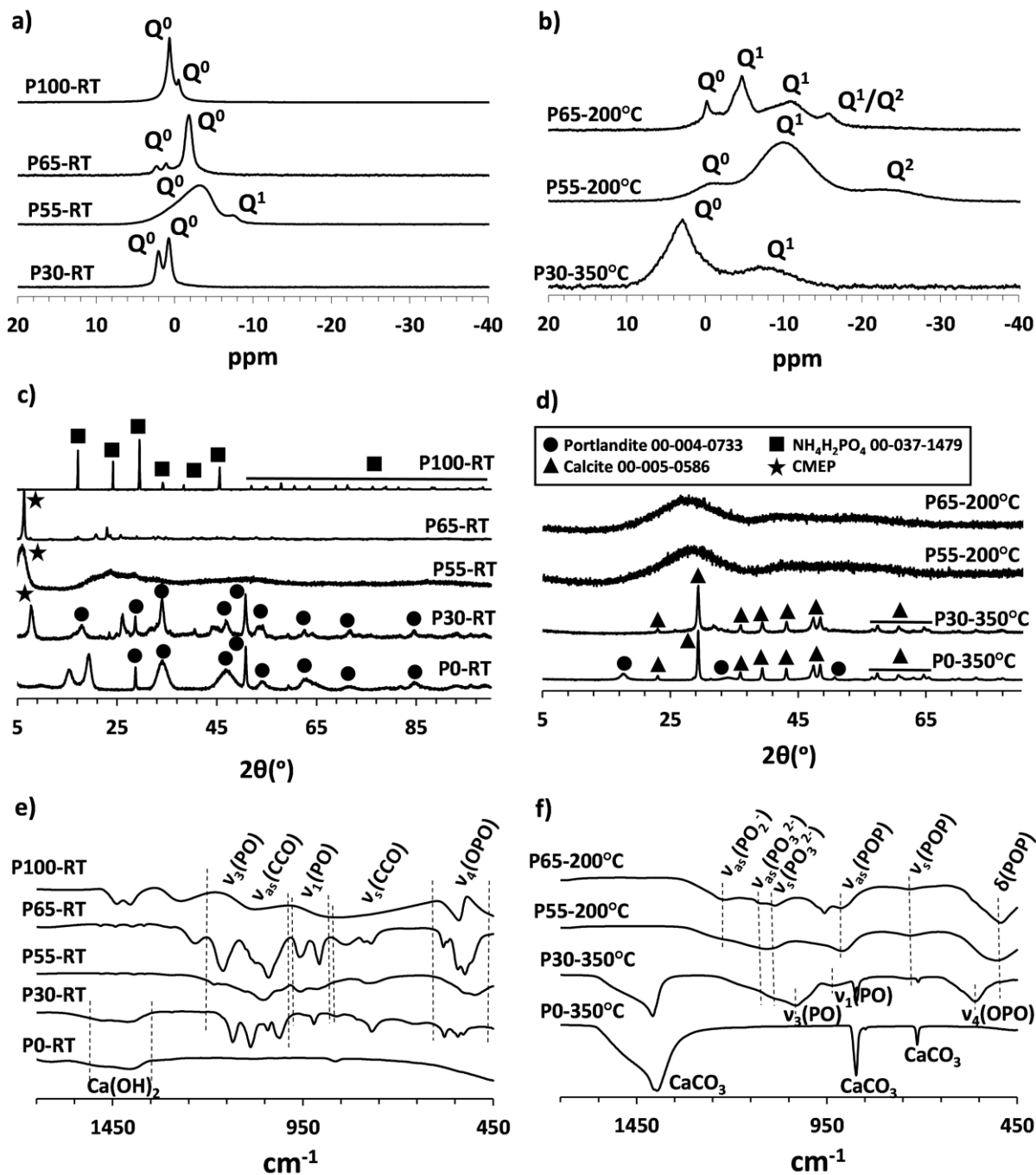
ACCEPTED MANUSCRIPT



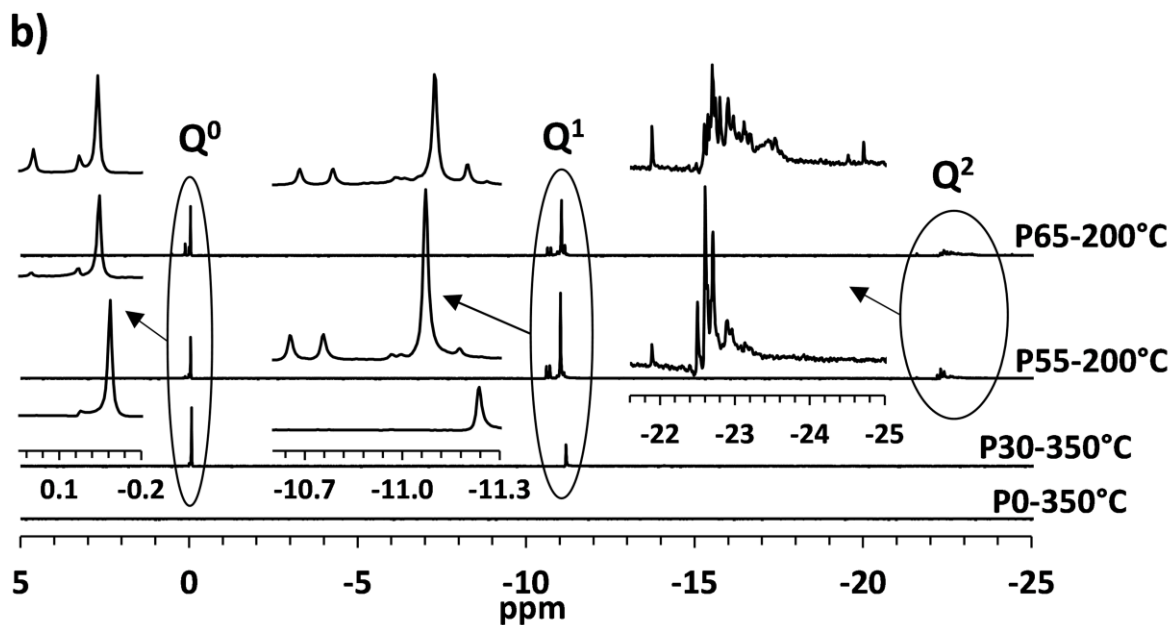
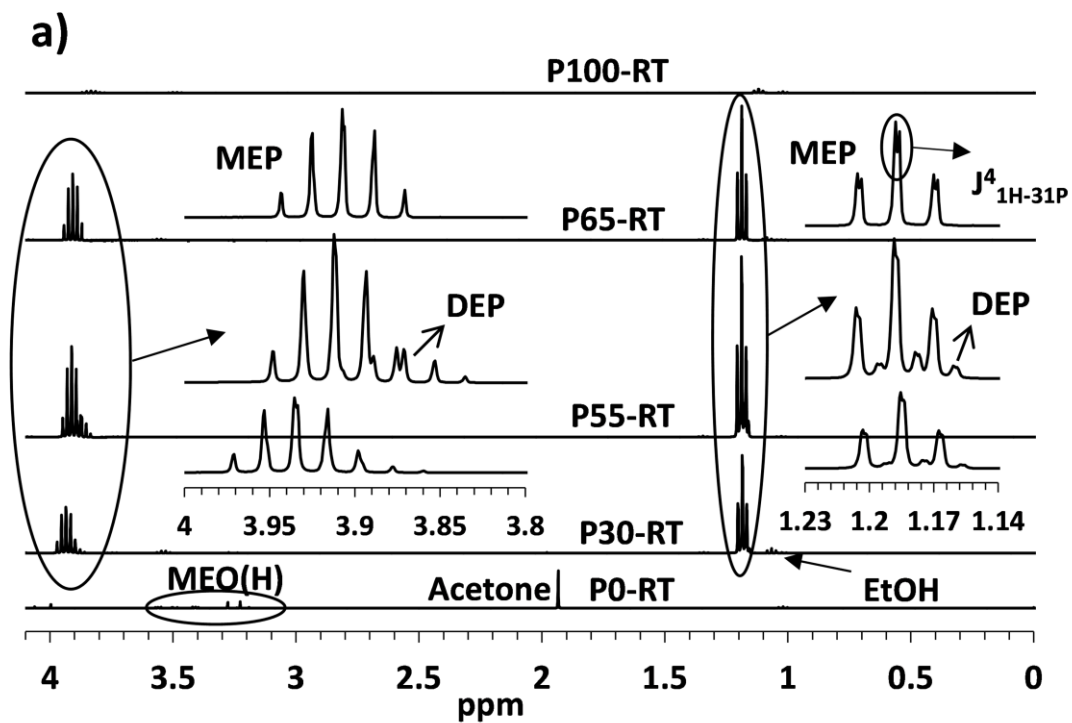
ACCEPTED

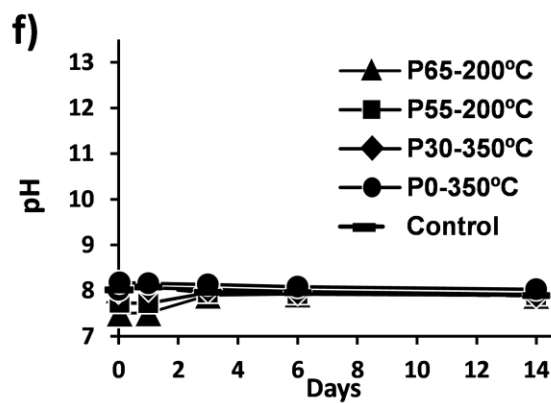
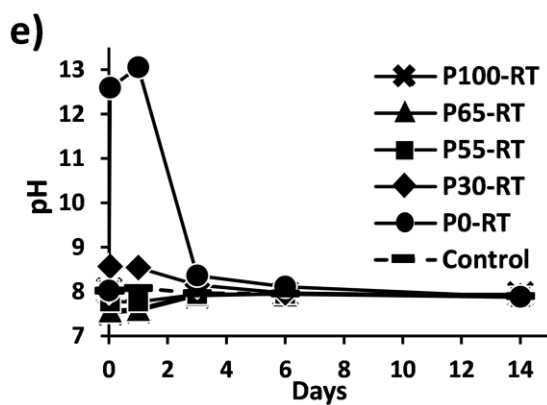
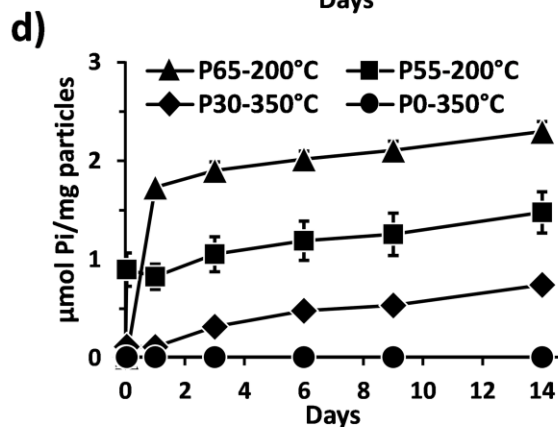
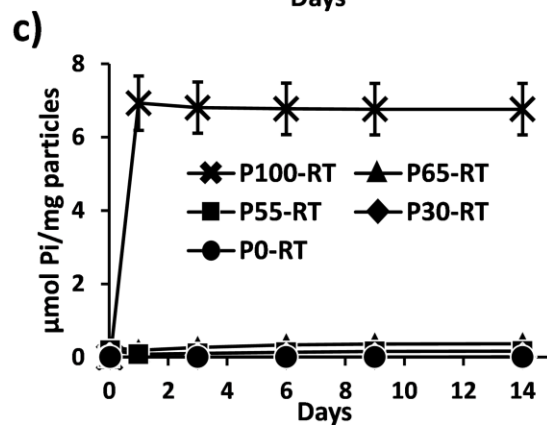
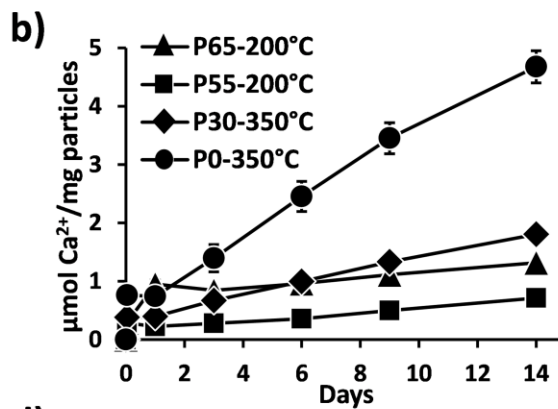
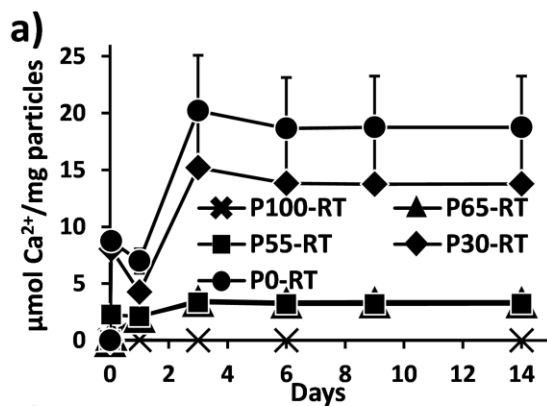


ACCEPTED

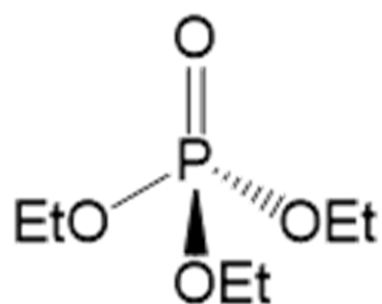
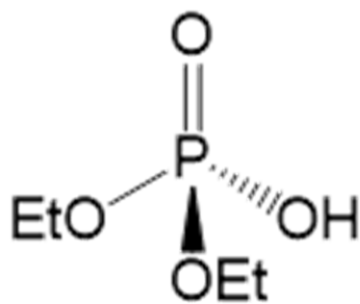
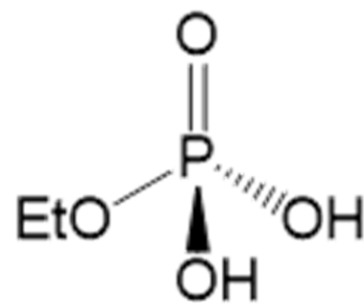
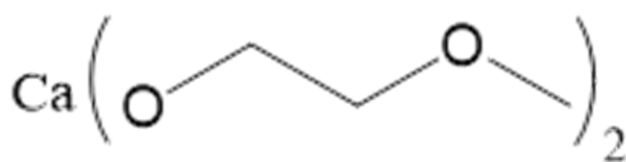


A





ACC

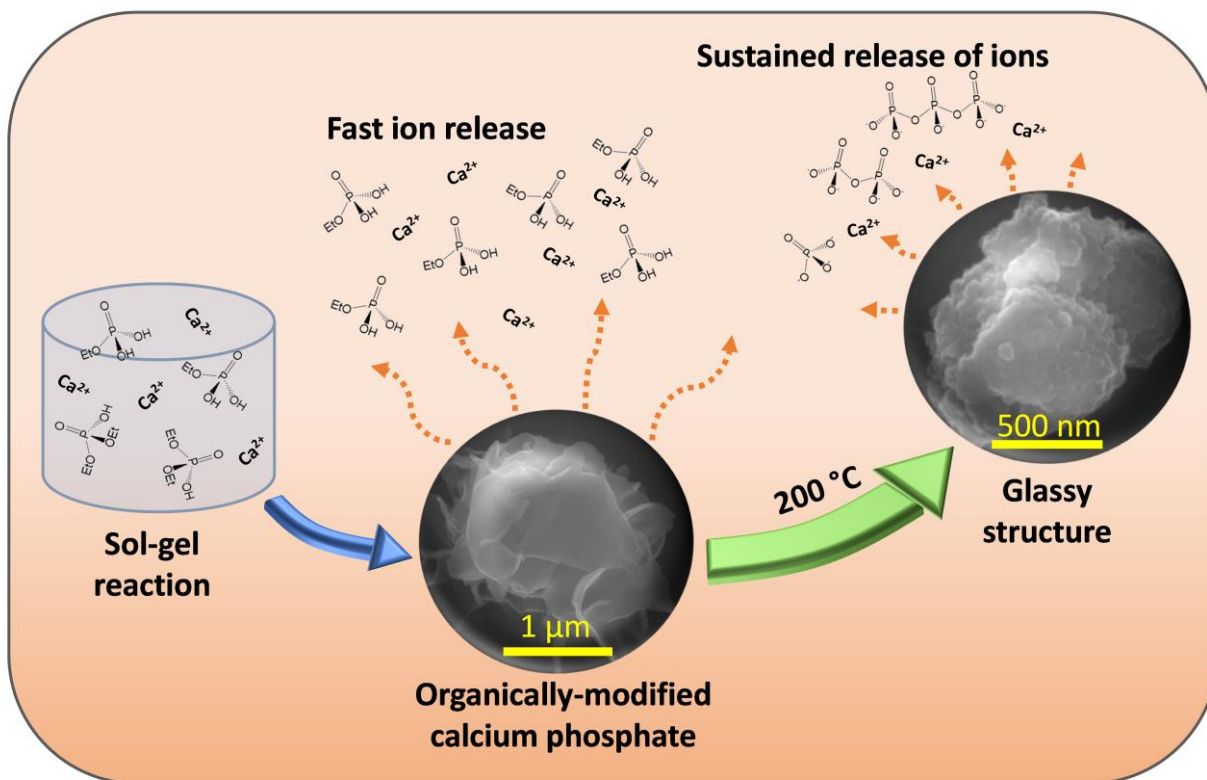
**TEP****DEP****MEP****CMEO**

ACCEPTED MANUSCRIPT

a)	P:Ca precursors (mL)	EtOH:NH ₃ :H ₂ O (mL)	Yield (mg)	Mass loss after thermal treatment (%)
P100	10:0	90:1.7:10	127	Decomposed (200 °C)
P65	8.5:1.5	90:1.9:6	359	-26.9 (200 °C)
P55	4:6	90:0:0	718	-25.96 (200 °C)
P30	1.5:8.5	90:30:0	948	-23.24 (350 °C)
P0	0:10	90:30:0	781	+19.59 (350 °C)

b)	P/Ca (atomic %)	C (mass %)	N (mass %)
P100-RT	100	0.80	12.63
P65-RT	63.9/36.1	17.13	≤0.2
P55-RT	54.2/45.8	15.81	≤0.2
P30-RT	28.7/71.3	9.77	≤0.2
P0-RT	0	3.15	≤0.2

c)	P/Ca (atomic %)	C (mass %)	N (mass %)
P100-200°C	Decomposed	Decomposed	Decomposed
P65-200°C	62.9/37.1	0.34	≤0.2
P55-200°C	56.5/43.5	0.37	≤0.2
P30-350°C	29.8/70.2	5.66	≤0.2
P0-350°C	0	7.74	≤0.2



ACCEPTED M